Experimental study of thermal lens features in laser ceramics

Alexander Soloviev*, Ilya Snetkov, Victor Zelenogorsky, Ilya Kozhevatov, Oleg Palashov, Efim Khazanov

The Institute of Applied Physics of the Russian Academy of Sciences,
46 Ul'yanov Street, 603950, Nizhny Novgorod, Russia
**Corresponding author: solo@appl.sci-nnov.ru*

Abstract: Thermal lens measurements were made by means of a high-accuracy phase shift interferometer that combines a $\lambda/1000$ sensitivity and 10 μm transverse resolution. The effect of random small-scale modulation in thermally induced phase distortion predicted earlier was proved experimentally. The statistical parameters of modulation were measured depending on heating power for two different ceramic samples. The experimental data agree well with results of numerical simulation.

OCIS codes: (110.3175) Interferometric imaging; (120.3180) Interferometry; (120.5050) Phase measurement; (120.6810) Thermal effects; (160.4670) Optical materials; (160.4760) Optical properties;

References and links

1. K. Ueda. "Ceramic lasers for IFE power plant" in *Proceedings of International Conference on Lasers, Applications, and Technologies*, St. Petersburg, p. LWG2 (*2005)*.
2. E. A. Khazanov, "Thermally induced birefringence in Nd:YAG ceramics," Opt. Lett. **27**, 716-718(2002).
3. M. A. Kagan and E. A. Khazanov, "Compensation for thermally induced birefringence in polycrystalline ceramic active elements," Quantum Electron **33**, 876-882(2003).
4. I. B. Mukhin, O. V. Palashov, E. A. Khazanov, A. Ikesue, and Y. L. Aung, "Experimental study of thermally induced depolarization in Nd:YAG ceramics," Opt. Express. **13**, 5983-5987(2005).
5. I. L. Snetkov, I. B. Mukhin, O. V. Palashov, and E. A. Khazanov, "Properties of a thermal lens in laser ceramics," Quantum Electron. **37**, 633-638 (2007).
6. I. L. Snetkov, A. A. Soloviev, and E. A. Khazanov, "Investigation of a thermal lens in thin disks of laser ceramics," Quantum Electron. (to be published).
7. V. V. Zelenogorsky, A. A. Solovyov, I. E. Kozhevatov, E. E. Kamenetsky, E. A. Rudenchik, O. V. Palashov, D. E. Silin, and E. A. Khazanov, "High-precision methods and devices for in situ measurements of thermally induced aberrations in optical elements," Appl. Opt. **45**, 4092-4101 (2006).
8. A.A. Soloviev, I.E. Kozhevatov, O.V. Palashov.E.A. Khazanov, "Compensation for thermally induced aberrations in optical elements by means of additional heating by CO_2 laser radiation," Quantum Electron. **36**, # 10, 939-945(2006)
9. P. Popov, K. Dukel'ski, I. Mironov, A. Smirnov, P. Smolyanski, P. Fedorov, V. Osiko, T. Basiev, "Thermal Conductivity of CaF_2 Optical Ceramic," Doklady Phys. **52**, 7-9 (2007).
10. O. V. Palashov, E. A. Khazanov, I. B. Mukhin, I. A. Mironov, A. N. Smirnov, K. V. Dukel'skii, P. P. Fedorov, V. V. Osiko, and T. T. Basiev, "Comparison of the optical parametersof a CaF_2 single crystal and optical ceramics" Quantum Electron. **37**, 27-28 (2007).
11. CaF_2 Product Information Sheet (Corning Incorporated, 2003). http://www.corning.com/docs/specialtymaterials/pisheets/H0607_CaF2_Product_Sheet.pdf
12. L. N. Soms and A. A. Tarasov, "Thermal deformation in color-center laser active elements. 1. Theoty," Sov. J. Quantum Electron. **9**, 1506-1508 (1979).
13. Data Sheet for Calcium Fluoride (SCHOTT Lithotec, 2006). http://www.us.schott.com/lithotec/english/download/caf2_june_2006_final_us.pdf
14. J. H. Burnett, "Stress-optical coefficients of 157 nm materials," Sematech 157 nm Tech. Data Rev., (Maryland, 2001) http://www.sematech.org/meetings/archives/litho/157/20011212/POSTER-Burnett-Metrology.pdf

1. Introduction

Recently, laser ceramics has become a serious challenge to crystalline optics because of its manufacturability and lower price. Ceramics is of particular interest for active elements in powerful lasers.

Cubic crystal ceramics is indistinguishable by its optical properties from analogous single crystals [1]. Nevertheless, in the presence of mechanical stress caused, for example, by inhomogeneous heating, the phase and depolarization distortions contain the inhomogeneities of grain size scale. This is due to the fact that in a strained single crystal the evolution of the transmitted irradiation depends on crystallographic axes orientation. Grains in ceramics have arbitrary orientation; hence, the distortion picture has a random character. The phase inhomogeneities deteriorate the beam irreparably and complicate focusing, and at high intensities may lead to filamentation due to self-focusing.

Arising of small-scale modulation in thermally induced distortions in ceramics was predicted in the work [2]. The statistical characteristics of depolarization were studied analytically in [3] and experimentally in [4]. In the papers [5,6], analytical expressions for statistical characteristics of phase distortions were obtained for different approximations (long rod, thin disk, weak heat sink, etc.); besides, numerical simulation for the more common case of cylindrical symmetry was done. However, these results have not been proved experimentally.

The current work is concerned with experimental investigation of thermally induced phase distortions of the radiation passed through the CaF_2 ceramics. The study was carried out by means of a phase-shift interferometer. The experimental setup is described in section 2. The results of measurements of statistical expectation and phase dispersion confirming the effect of small-scale inhomogeneities in thermal lens predicted earlier are presented in section 3.

2. Experimental setup

The measurements were done by means of the interferometer analogous to that described in the papers [7,8]. Special attention was focused on phase inhomogeneities with grain size scale (100-300 μm), for that purpose the interferometer optics was adjusted such that 1 pixel of CCD corresponded to ~10 μм in the plane of the sample. Thus, the sought inhomogeneities corresponded to some tens of pixels.

2.1 General scheme of experiment

The principal layout of the experiment is presented in Fig. 1. One can divide it into two functional parts. The first part (Fig. 1, elements from 1 to 11) forms the heating radiation. It consist of a heating CO_2 laser 1(10.6 μm wavelength); semitransparent NaCl mirror 2 that branches off part of radiation to the bolometric power meter 3, a couple of spherical mirrors 4 and 5 that allow one to control the radius of a heating beam, and chopper 6 that controls average power. For simplification of the setup adjustment laser diode 7 was used, the radiation from which at the wavelength of 650 nm was superposed at the salt mirror 2 with CO_2 laser irradiation.

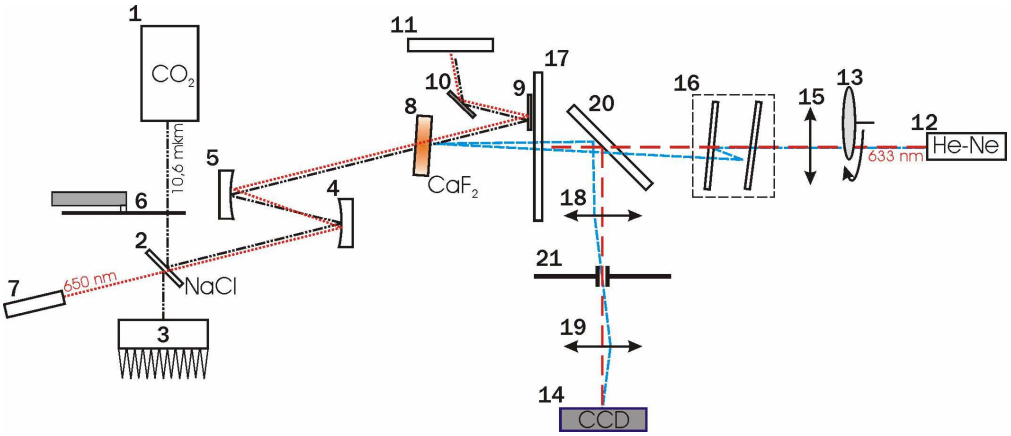

Fig. 1. Scheme of experimental setup : 1 – CO_2 laser, 2 –semitransparent salt wedge, 3 – power meter, 4-5 – spherical mirrors, 6 –chopper, 7 – alignment diode source, 8 – sample under study, 9-10 metallic mirrors, 11 – absorber, 12 – probe radiation source, 13 – speckle fission unit , 14 – CCD-camera, 15, 18, 19 – lenses, 16 –wave front conjugation unit, 17 – reference plate, 20 – semitransparent mirror, 21 – aperture

The CO_2 laser beam of Gaussian shape was incident on sample 8 at a small angle. We rejected normal incidence to avoid heating of interferometer by CO_2 laser radiation. For the same reason we used metallic reflectors 9, 10 and absorber 11. Ceramic and single crystalline wedge plates 3 mm and 3.5 mm thick with a radius of 7 mm were studied in the experiments. We used the wedge plates to separate phase distortions or probe radiation reflected from the different faces of the sample. For 10.6 μm wavelength radiation, the absorption depth is close to 3 mm, which for our 3.5 mm sample corresponds to the transmission of 25% and absorption of 70% of incident power. In the majority of the experiments the heating was produced by a beam 2 mm in diameter.

The second part of the layout (elements from 12 to 21) has a measuring function – it is a high accuracy phase-shift interferometer. The radiation of the probe He-Ne laser 12 gets to the speckle fission unit 13, that it described in more detail in section 2.3. The speckle fission unit is in the focus of the objective 15, where the radiation is collimated. Further, the radiation goes to the conjugation unit 16 [7,8] consisting of two semitransparent mirrors. These mirrors serve to superpose the interfering beams in space and to modulate the path-length by moving one of the mirrors. Only two beams emitted from the conjugation unit 16 are used in the scheme: the transmitted beam and the beam twice reflected from the mirrors of the conjugation unit. These beams must reflect from the surface of sample 8 and reference plate 17, respectively. Indeed, depending on whether the front or the rear surface is utilized for interference one can obtain information about the surface or about the bulk of the sample (see section 2.4). The lenses 18 and 19 transfer the image of the sample surface under study to the CCD matrix, taking into account the reflection in the semitransparent mirror 20. The aperture 21 provides angular filtration of parasitic reflections which are produced in optical scheme elements. It is important to note that, thanks to its unique design and original calculation algorithm, the interferometer permits phase distortion measurements to an accuracy up to $\lambda/1000$ [7]

2.2 The spatial resolution of the interferometer

The main characteristic feature of the presented experimental layout consists in a combination of two properties: high sensitivity to phase distortions (<1 nm) and high resolution (~10 μm). The problems of small distortions measurements and high resolution imaging are generally solved separately. Moreover, for high sensitivity interferometers (Fizeau interferometer) the requirements of high sensitivity and high transversal resolution are contradictory.

Indeed, to ensure high resolution ($\Delta x \to 0$), the optical scheme must transmit radiation with angular spectrum $\Delta\Omega$:

$$\Delta\Omega = \frac{\lambda}{\Delta x}. \quad (1)$$

However, another relation holds in interferometer:

$$\Delta\Omega \frac{d}{\lambda} \le 2\pi, \quad (2)$$

where d is the optical path difference between the interfering beams. For fixed path difference d, the increase of measurement accuracy demands increasing the signal/noise ratio in conformity with contrast enhancement. This requirement is fulfilled the better, the better the condition Eq. (2) is fulfilled, i.e., for $\Delta\Omega \to 0$.

Thus, the increase of resolution requires angular spectrum widening, which contradicts contrast enhancement and, hence, sensitivity of interferometer. The scheme in Fig. 1 with conjugation unit 16 removes this contradiction since the equivalent path difference of interfering beams is close to zero. Consequently, the angular spectrum width $\Delta\Omega$ can be enlarged in conformity with the requirement Eq. (1) without damage to the requirement Eq. (2). Besides, the part of the scheme that transfers the image of the studied surface consist of two lenses 18 and 19. The surface under study is placed in the focal projection plane of lens 18, the geometrical aberrations in which are minimized for transferring the image to 'infinity', while the image in the plane of CCD matrix is constructed by lens 19 well corrected to obtain an image from the infinity. Such a combination of lenses is good as it allows easy coordination of the scales of the source (2 mm) and the image (5 mm). For this it suffices that the ratio of the focal lengths of the objectives be equal to 5/2. Moreover, it allows one to sort the angular spectrum by means of the aperture 21.

As a result the scheme in Fig. 1 combines two features that are of fundamental importance for experiment: high transversal resolution (~10 μm) and high sensitivity (λ/1000).

2.3 Speckle fission unit

The conducted interferometric measurements of phase make use of the intensity distribution from a CCD-camera (14 in Fig. 1). However, high coherence of the probe radiation source gives rise to strong alternating inhomogeneities (speckles) that are superposed on the intensity distribution under consideration, thus making interferometric measurements almost unfeasible. For reducing speckle amplitude in the intensity distribution we used a round dispersive plate through the edge of which the radiation of He-Ne laser12 passed. By rotating the plate around its center we introduced time-depended chaotic phase distortions in probe radiation, which led to strong rebuilding of speckle picture in the CCD-camera. The speckles were averaged over frame exposure time. But the presence of time-dependent chaotic intensity variations in the CCD-camera led to strongly noisy (from frame to frame) recorded intensity, even at highly stable He-Ne laser power. This phenomenon had a negative influence on phase measurements accuracy since reconstruction of phase distribution demands processing of a series of consecutive frames from the camera.

Speckle averaging may be improved by increasing rotation speed of the fission unit plate. However, the high speeds of rotation led to vibrations in the mechanism of plate fastening, which was observed in the time spectrum of radiation intensity recorded by the CCD-camera.

The regime of matched frame repetition rate (25 fps) and plate rotation period (40 ms) proved to be optimal. The sequence of intensity fluctuations averaged in each frame was the same, and the plate rotation frequency of the fission unit was sufficient for the speckle averaging to the level that is lower than the measuring accuracy of the used 8-bit camera. The described regime of synchronization allowed us to reduce the intensity noise and get rid of

resonance peaks in the time spectrum. The use of such an approach provided a twice better accuracy of phase registration

2.4 Interference scheme variants

We now consider in more detail possible variants of the interference scheme (Fig. 2).

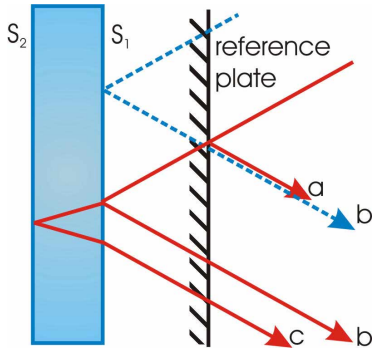

Fig. 2. Possible variants of interferometric measurements. S1 and S2 are sample surfaces. Doubled incident beam is presented with red solid and blue dashed lines. The reflections of the probe beam are marked by the following characters: a – from the reference plate, b – from the front surface, c – from the rear surface.

A lot of reflections appear in the system consisting of a reference plate and sample surfaces when a probe beam is incident on them. Consider three reflected beams labeled by (a), (b) and (c) in Fig. 2. Incident beam is multiple since it is doubled by the conjugation unit (16 in Fig. 1) to stimulate interference. Different physical quantities may be measured, depending on the pair of reflections which is interfering. When the [a,b] pair is superposed (shown in Fig. 2), the interference pattern contains information about front surface distortions. By superposing the [c,b] pair (not shown in Fig. 2), we will measure the quantity that may be written, neglecting beam deflection from the straight trajectory, as:

$$\Delta L(z) = \int_0^l \left[n_0 \left(\Delta S_1(z) + \Delta S_2(z) \right) + \beta T(z) + \Delta_n(z) \right] dz \,, \tag{3}$$

where l is the thickness of the sample; n_0 is the unperturbed refractive index; T denotes temperature, β = dn/dT, Δ_n is the term responsible for the photoelastic effect, which strictly speaking depends on polarization; and ΔS_1 and ΔS_2 are geometrical displacements of the sample surfaces along the outer normal due to heating.

The quantity that is measured when the [a,c] pair (not shown in Fig. 2) is used may be written in the form

$$\Delta L = \int_0^l \left[(n_0 - 1)\Delta S_1 + n_0 \Delta S_2 + \beta T(z) + \Delta_n(z) \right] dz \tag{4}$$

In our work we used the variants where the [a,c] and [a,b] pairs were superposed the combination of which allowed us to partially separate the bulk and the surface heat distortions in the studied sample.

Below the measurements made for the [a,b] pair will be called surface measurements, and for the [a,c] pair bulk measurements.

3. Results of the measurements

Two ceramic and one single crystalline CaF_2 samples synthesized and studied in [9,10] were investigated: the first one was a cylinder with the radius of 7 mm and thickness of 3.5 mm, the second sample was rectangular (12x14 mm) with the thickness of 3 mm. A single crystalline plate having dimensions 12x14x1.5 mm was investigated as well.

3.1 The 'cold' measurements

At the first stage, the bulk and surface inhomogeneities of the ceramics were measured in the absence of heating radiation. These inhomogeneities will be referred to as 'cold' phase distortions. Aberrations of the probe radiation in the sample at CO_2 laser heating will be called 'hot' phase distortions. Typical 'cold' profiles are presented in Fig. 3.

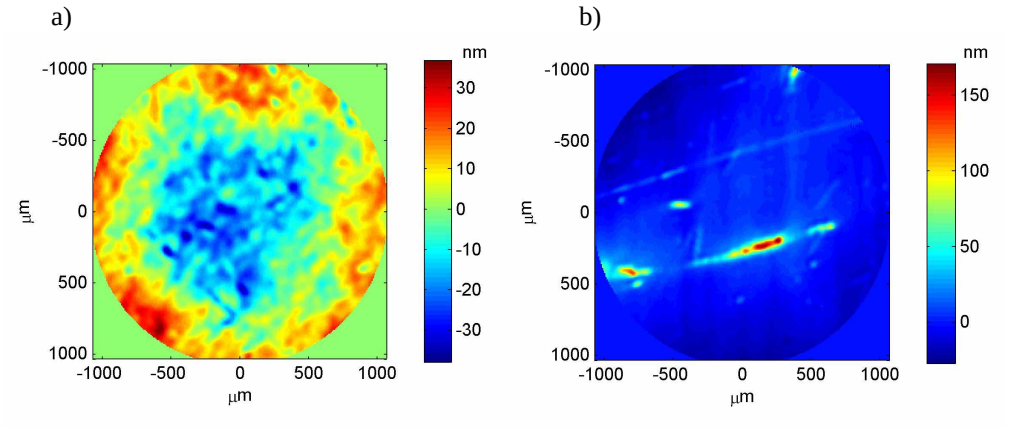

Fig. 3. Typical 'cold' profiles of the ceramic sample at bulk a) and surface b) measurements.

One can see in the figure both types of inhomogeneities, large (lens) and small, comparable with grain size. All inhomogeneities are connected with the imperfection of production technologies. The ceramics surface Fig. 3(b) contains a 150 nm scratch that is connected with polish defect of naturally soft CaF_2. Nevertheless these initial ingomogeneties (including scratch) are not essential because we interested in differential picture of phase distortions.

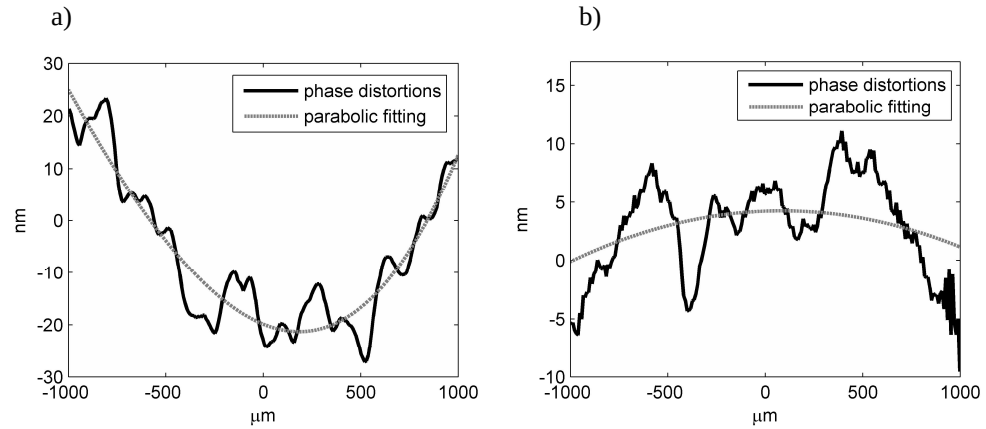

Fig. 4. Crossections of typical 'cold' profiles of the ceramic sample at bulk a) and surface b) measurements with the parabolic fitting superpose.

If a parabola is superposed (in sense of STD minimization, here and below STD is standard deviation) on the cold distortion profile obtained in experiment (Fig. 4), then a standard deviation from this parabolic approximation will be about 5 nm for the surface and 10 nm for the bulk measurements. For the surface measurement this quantity characterizes surface roughness, and for the bulk measurements, refractive index inhomogeneity in combination with surface roughness (see section 2.4). In our scheme it is impossible to directly measure inhomogeneity of the refractive index, but one can estimate it assuming statistical independence of bulk and surface inhomogeneities. This estimate gives 6 nm for the refractive index inhomogeneity.

3.2 Linearity of distortions as a function of heating power

The differential picture, i.e., the arithmetic difference of 'hot' and 'cold' phase distortions in the same area of the sample is of major interest in studies of thermal distortions. This difference will be called below 'differential' distortions. It was shown experimentally and numerically (the used numerical code [6] took into account the dependence of heat generation on the longitudinal coordinate) that one can conventionally distinguish two temporal scales. The first scale is connected with setting up of the temperature profile – the difference between the highest and lowest temperature. It can be estimated as $\rho C_p W^2/\kappa$; where ρ is density, C_p is heat capacity, W is the size of heat source, κ - thermal conductivity and for CaF_2 is about 1 sec. The second scale is associated with the increase of mean temperature in the sample; it is determined by heat capacity of the medium and heat transfer conditions. In case of weak convective heat sink that was actualized in our experiments the second scale is tens of minutes. It was experimentally shown that in 10 seconds after heating started the changes of phase distortions during the measuring time (1/2 sec) were below the accuracy of the measurements. Therefore, all hot measurements of thermal distortions were made not earlier than 20 seconds after heating start, when the temperature profile has, actually, set up.

First of all we studied the differential distortions as a function of heating power. The differential distortions increase in amplitude with increasing heating power but their shape remains invariable, including small-scale modulation (see section 3.3). The optical power of a large-scale thermolens 1/F as a function of heating power is plotted in Fig. 4. The dn/dT in CaF_2 is negative but its contribution is compensated by surface deformation therefore the probe radiation reflected from the rear face (reflection (c) in Fig. 2) is integrally focused as distinct from front face reflection (reflection (b) in Fig. 2).

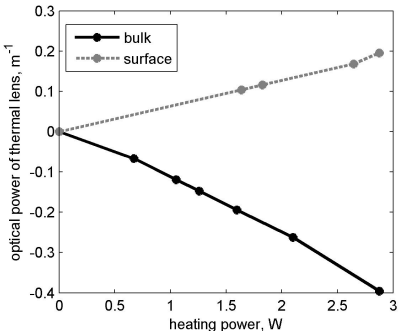

Fig. 5. The dependence of thermally induced thermolens in ceramics on heating power for bulk (solid line) and surface (dash line) measurements.

Note that in the case of surface measurements, the differential distortions do not contain small-scale modulations, i.e. they remain smooth.

According to [11], the characteristics of CaF_2 such as β, heat conductivity, photoelastic constants, etc. depend appreciably on temperature. Therefore, it is hard to predict behavior of the medium at considerable heating. Numerical modeling of a non-stationary heat conduction

equation shows that the temperature in the sample can raise by hundreds of degrees. The insignificant bending of the graphs in Fig. 5 is a consequence of medium constants temperature dependence.

We compared the experimental phase distortions with results of numerical modeling. For the surface distortions, the coincidence proved to be good. For the bulk measurements, the theoretically predicted the optical power of thermal lens is about 2.5 times higher than the experimental one. We attribute such a deflection to inaccuracy of determining CaF_2 constants. In particular, we found two sets of photoelastic constants, data in which differ significantly. The first set was mentioned in the paper [12], the second in the papers [11,13,14]. It would be noted that in CaF_2 distortions caused by dn/dT and the photoelastic effect are partially compensated by surface displacement, which leads to high sensitivity of total distortions to the material constants of the medium.

3.3 Dispersion of thermally induced phase distortions

As was mentioned above, the important distinctive feature of the behavior of mechanically stressed ceramics as compared to genuine isotropic media is small-scale inhomogeneity of phase distortions of transmitted radiation [5].

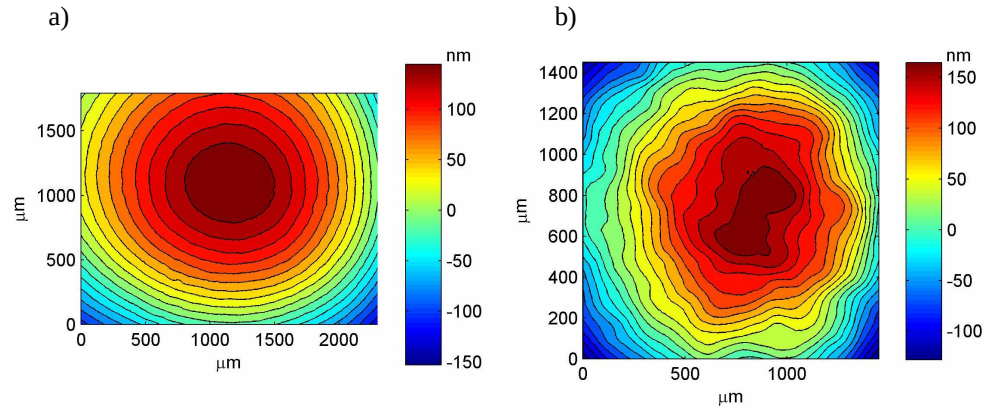

Fig. 6. Differential phase distortions in single crystalline (a) and ceramic (b) element at bulk measurements.

For comparison, typical pictures of differential distortions in a single crystal and a ceramic sample caused by bulk heating are presented in Fig. 6. The distortions in the single crystal (Fig. 6(a)) are smooth in contrast to the ceramics, where one can see inhomogeneities with hundreds of microns scale without extra processing (Fig. 6(b)).

For quantitative assessment of phase inhomogeneities and dispersion measurements the fourth-order surface was superposed on the profile of the differential distortions in sense of minimization of the STD. Below, we will refer to the STD obtained in this way as to experimental STD.

This procedure is meaningful because in 10 seconds after heating start the temperature in the crystalline or ceramic CaF_2 sample is smooth by virtue of relatively high thermal conductivity and can not contain hundreds of micron scale inhomogeneities inside. Thus, all small-scale inhomogeneities are associated with the ceramics nature of the studied sample. This statement is confirmed by the fact that experimental distortions in the single crystal are excellently approximated by the fourth-order surface.

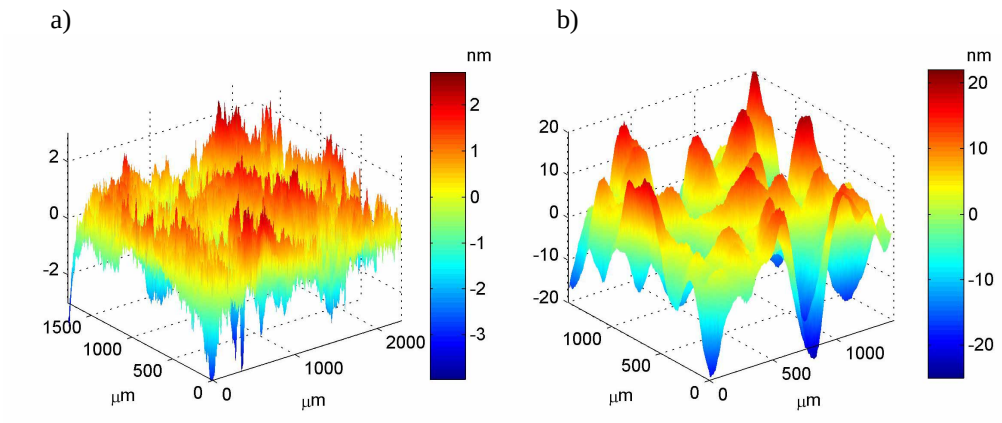

Fig. 7. The differences of distortions presented on the Fig. 6 from smooth 4-th degree approximations for single crystal (a) and for ceramics (b).

The difference of distortions in the single crystal from their approximation (Fig. 7(a)) has a noise nature and is due to measurement error. The experimental STD is independent of heating power and its magnitude is less than one nanometer, which is close to the accuracy of the used interferometer (λ/1000).

After subtracting the smooth fourth-order approximation (Fig. 7(b)), the phase distortions in ceramics have pronounced inhomogeneities with hundreds of microns transverse scale and STD of about 10 nm.

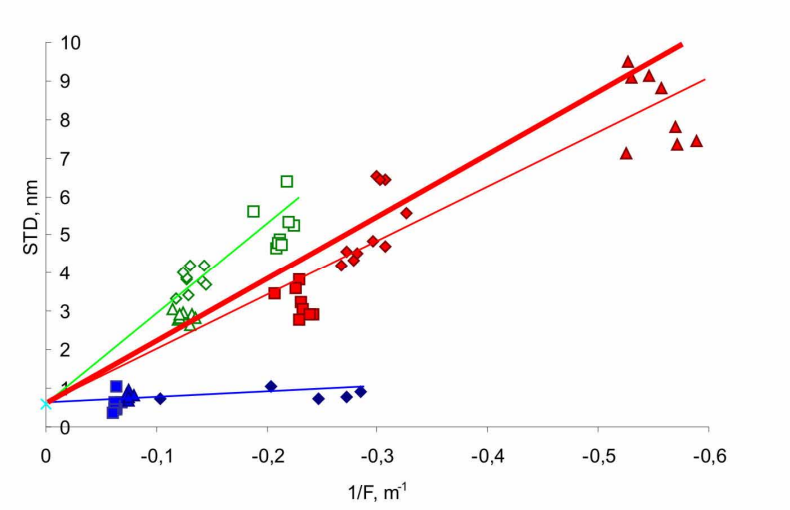

Fig. 8. The dependence of experimental STD on 1/F of the corresponding thermolens. The linear approximation is plotted by a thin blue solid line for the single crystal, by red and green thin solid lines for the 3.5 mm-thick and 3 mm thick ceramic elements, respectively. The thick red solid line corresponds to numerical modeling. The approximating lines originate from point [0;0,6] that corresponds to measurement accuracy (λ/1000).

Then, we measured the STD in different regions of the sample aperture (the sample was moved transversely to the probe beam of interferometer by the distance comparable with the grain size) for different power of heat generation (Fig. 8). One point on the graph represents one differential measurement. The optical power of a large-scale thermolens 1/F proportional to the total power of heat generation is laid off on the horizontal axis. The points of the same

shape correspond to the same power of the heating CO_2 laser. Because of inhomogeneity of absorption they have a slightly different thermolens.

The linear approximations of the experimental points in the plot are represented by the thin solid lines. The red thick solid line corresponds to the STD obtained numerically for the ceramic sample of 3 mm thickness with 100 μm characteristic grain size (we used the set of constants for CaF_2 from [13]). The calculations were made by means of numerical code described in works [6-8]. A good agreement with experimental data is clearly seen in Fig. 8.

As is seen from Fig. 7, STD is proportional to 1/F for each ceramic sample, which agrees with theoretical predictions [5]. STD in a single crystal does not depend on heating power and is significantly less than in ceramics. Hence, we can state that the accuracy of the used interferometer is sufficient for measuring thermally induced phase distortion inhomogeneities in ceramics.

4. Conclusion

To the best of our knowledge we obtained a pioneer confirmation of the effect of small-scale modulation of thermally induced phase distortions in laser ceramics. The effect was demonstrated on an example of CaF_2 ceramics with a characteristic grain size of 100 μm. A good quantitative agreement with results of numerical modeling was obtained.

In full conformity with the theoretical predictions, the scale of the small-scale modulation is close to the characteristic grain size and STD of these inhomogeneities linearly depends on heating power. To reduce this negative effect, one should increase the number of grains on the beam path (the sample length to grain size ratio).

The measurements were performed by means of a high accuracy phase-shift interferometer that combines 10 μm spatial resolution and λ/1000 sensitivity. To improve accuracy, mechanical speckle splitter synchronized with a CCD camera was used.